Blueshift and intramolecular tunneling of NH[sub 3] umbrella mode in [sup 4]He[sub n] clusters

Alexandra Viel, K. Birgitta Whaley, Richard J. Wheatley

Blueshift and intramolecular tunneling of N H 3 umbrella mode in He n 4 clusters

Alexandra Viel, K. Birgitta Whaley, and Richard J. Wheatley

Citation: The Journal of Chemical Physics **127**, 194303 (2007); doi: 10.1063/1.2787004
View online: http://dx.doi.org/10.1063/1.2787004
View Table of Contents: http://scitation.aip.org/content/aip/journal/jcp/127/19?ver=pdfcov
Published by the AIP Publishing

Blueshift and intramolecular tunneling of NH_3 umbrella mode in ^4He_n clusters

Alexandra Viel[a)]
Kenneth S. Pitzer Center for Theoretical Chemistry, Department of Chemistry, University of California, Berkeley, California 94720-1460, USA and Laboratoire de Physique des Atomes, Lasers, Molécules et Surfaces (PALMS), UMR 6627 du CNRS, Université de Rennes 1, Campus de Beaulieu, F-35042 Rennes, France

K. Birgitta Whaley[b)]
Kenneth S. Pitzer Center for Theoretical Chemistry, Department of Chemistry, University of California, Berkeley, California 94720-1460, USA

Richard J. Wheatley
School of Chemistry, University of Nottingham, University Park, Nottingham NG7 2RD, United Kingdom

(Received 15 May 2006; accepted 28 August 2007; published online 16 November 2007)

We present diffusion Monte Carlo calculations of the ground and first excited vibrational states of NH_3 ^4He_n for $n \leqslant 40$. We use the potential energy surface developed by one of us [M. P. Hodges and R. J. Wheatley, J. Chem. Phys. **114**, 8836 (2001)], which includes the umbrella mode coordinate of NH_3. Using quantum Monte Carlo calculations of excited states, we show that this potential is able to reproduce qualitatively the experimentally observed effects of the helium environment, namely, a blueshift of the umbrella mode frequency and a reduction of the tunneling splittings in ground and first excited vibrational states of the molecule. These basic features are found to result regardless of whether dynamical approximations or exact calculations are employed. © *2007 American Institute of Physics*. [DOI: 10.1063/1.2787004]

I. INTRODUCTION

The recent rise in interest in the study of doped helium clusters derives from the realization that such systems can provide information both on the dopant in a quantum solvation environment and on a superfluid helium environment at molecular length scales. Infrared (IR) spectroscopy of molecules embedded inside ^4He allows one to look at the effect of a weakly interacting Bose quantum liquid environment on vibrational and rotational properties of the molecule.[1–3] A great deal of attention has focused on the measurement and analysis of the rotational dynamics of molecules in helium.[3–5] Changes in the vibrational properties induced by helium are less well studied, as also the modification of intramolecular and intermolecular tunneling splittings in molecules and complexes solvated by helium. In most cases, the measured vibrational frequency shifts are found to be small, i.e., of the order of a few cm^{-1} or less. For example, the ν_3 vibration frequencies of SF_6 (Ref. 6) and of OCS (Refs. 7 and 8) are shifted by -1.4 and by -0.92 cm^{-1}, respectively, and the stretch of HF by -2.65 cm^{-1} (Ref. 9) or -2.85 cm^{-1} (Ref. 10). Most shifts observed in the infrared are also to the red, reflecting the predominance of attractive forces on the overall magnitude of the vibrational shift within a given electronic state.[2,3] Tunneling splittings deriving from internal rotation modes have been measured in small water complexes in helium droplets and found to be unaffected by the helium environment.[11] In contrast, interchange tunneling splittings involving intermolecular modes in van der Waals complexes are generally found to be significantly quenched inside the droplets.[12,13] For the HF dimer, $(HF)_2$, a large fraction (74%) of the reduction in hydrogen interchange tunneling splitting in large helium droplets could be reproduced by fixed node diffusion Monte Carlo calculations in small clusters (ten helium atoms and less).[14] In this relatively rigid dimer situation, the tunneling path has high symmetry which is not broken by the presence of a small number of solvating helium atoms, and a fixed node calculation is appropriate. These calculations have recently been extended to larger sizes ($n=30$) and to also treat the HCl dimer.[15] For larger sizes where the helium solvation is no longer restricted to the equatorial plane of the dimer, the use of a fixed node approximation may be less accurate.

The vibrational dynamics of the ammonia molecule presents an example of intramolecular tunneling where the tunneling pathway couples two minima of a large amplitude motion, the umbrella mode of the NH_3 molecule. Such a large amplitude motion might be expected to be strongly affected by solvation with helium atoms, unlike the situation of internal rotation tunneling dynamics in Ref. 11. Two experimental groups have studied the rotationally resolved IR spectroscopy of ammonia trapped in cold ^4He clusters.[16,17] The earlier work measured the ν_2 vibrational mode directly with a line tunable CO_2 laser and concluded that an unusually large interaction between the host cluster and the umbrella motion of the NH_3 molecule existed, giving rise to a blueshift of 17.5 cm^{-1}, and reductions in tunneling constants by 75% and 30% in the ground and first excited states of the

[a)]Electronic mail: alexandra.viel@univ-rennes1.fr
[b)]Electronic mail: whaley@berkeley.edu

umbrella mode, respectively. This first set of measurements also yielded an estimate of a reduction in the rotational constant B by 24% from its gas phase value of 9.9 cm^{-1}. This last feature made NH_3 somewhat exceptional among light rotors ($B>1$ cm^{-1}), for which generally the rotational constants appear to decrease by only a few percent, if at all, in helium droplets.[3,5] The more recent experimental work[17] made an indirect estimate of the vibrational shift and tunneling splittings of the ν_2 mode based on high resolution measurements of the rovibrational spectra of the ν_1, ν_3, and ν_4 modes in helium droplets. These experiments yielded a significantly smaller estimate of the blueshift for the ν_2 mode, namely, 2.1 cm^{-1}, smaller changes in the tunneling splitting values, namely, to (101 ± 6)% and (94 ± 3)% of the gas phase values in the ground and first excited umbrella mode states, respectively, and a smaller reduction in rotational constant, to 95% of its gas phase value. (See also Ref. 18.)

These newer measurements suggest a weak but nontrivial effect of helium solvation on the NH_3 umbrella mode. One of the present authors has developed an intermolecular potential for the interaction between ammonia and helium that includes the dependence on the ammonia inversion tunneling coordinate.[19] In this potential, the location of the global minimum for the helium atom changes as the ammonia umbrella closes, moving from an equatorial location that is equidistant from the two closest hydrogen atoms when the NH_3 is planar, to an axial location on the same side as the hydrogen atoms when the NH_3 is pyramidalized. We show here that the associated change in shape of the $He-NH_3$ complex along the umbrella coordinate results in a blueshift of the umbrella vibrational mode and in a reduction of the tunneling splittings in both ground and excited states. The values of the blueshift and tunneling splittings are in good agreement with the more recent experimental results of Ref. 17 and are significantly smaller than the values extracted from the earlier experiments of Ref. 16. In this paper, we give first a static analysis of the interaction potential surface that provides qualitative insight into these features. We then present dynamical calculations for the excited states that incorporate all relevant nuclear motions, namely, the NH_3 umbrella inversion and the relative motions between NH_3 and the n helium atoms of the cluster. These allow the vibrational shift and tunneling splittings in ground and first excited states of the umbrella mode to be calculated. We present results from two different dynamical approximations and compare these with full dimensional calculations. We explicitly consider here clusters containing up to 40 helium atoms and extrapolate our results to compare with the experiments on large helium droplets.

The remainder of the paper is organized as follows. Section II outlines the theoretical approaches employed here for solving the Schrödinger equation for nuclear motion, including two different approximations based on different choices of time scale separation amongst the three relevant time scales and a direct approach made without any dynamical approximations. Section III presents results derived from each of these approaches for both the blueshift of the umbrella mode and for the reduction of the tunneling splittings. We assess these results by comparison with experiment and provide suggestions for further improvement in Sec. IV.

II. THEORETICAL APPROACH

A. Description of the system

The experimentally observed umbrella mode frequency[16,17] is defined as

$$\nu_2 = \frac{E_4 + E_3}{2} - \frac{E_2 + E_1}{2}, \tag{1}$$

where E_m refers to the first four energy levels of the double well potential corresponding to the umbrella (inversion) mode of NH_3. It is thus the difference between the tunneling-averaged ground and first excited vibrational state energies. The tunneling splittings in the ground state and excited vibrational states are given by the differences between symmetric and antisymmetric levels:

$$\delta_0 = E_2 - E_1, \tag{2}$$

$$\delta_1 = E_4 - E_3. \tag{3}$$

The helium environment perturbs the NH_3 molecule, leading to a shift in all three quantities, ν_2, δ_0, and δ_1. The large experimental blueshift of ν_2 by 17.4 cm^{-1} measured in 1998 (Ref. 16) was not confirmed by the recent experiment in Ref. 17, which instead revised this value down to 2.1 cm^{-1}. The large reductions of the tunneling splittings measured in Ref. 16 (from $\delta_o=0.79$ cm^{-1} and $\delta_1=35.7$ cm^{-1} in the gas phase down to $\tilde{\delta}_o=0.2\pm0.1$ cm^{-1} and $\tilde{\delta}_1=24.6\pm1$ cm^{-1} in helium) were also revised to significantly smaller reductions of 6% or less by the more recent experiments. These values, both vibrational shift and tunneling splittings, were obtained indirectly from the analysis of the rovibrational spectra of other vibrational modes and then reassigning the spectra of Ref. 16. This procedure yielded tunneling splitting values $\tilde{\delta}_o=0.8$ cm^{-1} and $\tilde{\delta}_1=33.7$ cm^{-1}. These experimentally obtained tunneling splittings were measured as the tunneling splittings of the $j=1$, $k=1$ NH_3 rotational state, i.e., the energy difference between the symmetric and antisymmetric states of the inversion coordinate. For the lowest rotational state, $j=0$, $k=0$, only the antisymmetric state is allowed, the symmetric tunneling state being forbidden by the permutation symmetry of the three nuclear spin 1/2 hydrogen atoms.[20]

In principle, computational determination of the blueshift and the tunneling splittings involves the calculation of excited states of a system with a large number of degrees of freedom. It is well known that Monte Carlo techniques are robust for ground state computations. Excited states can be calculated by these methods within the fixed node approximation[21] or, in many instances, by the projection operator imaginary time spectral evolution (POITSE) approach.[22–24] The latter does not rely on any assumptions concerning the position of the nodal surface, but it is computationally considerably more expensive to implement. We undertake POITSE calculations here but also explore two approaches involving different choices of time scale separa-

tions that allow the quantities ν_2, δ_0, and δ_1 to be evaluated using only ground state techniques. We therefore evaluate the tunneling splittings δ_0 and δ_1 for the lowest rotational state $j=0$, $k=0$, neglecting the effects of permutation symmetry of the H_3 unit. Given the small rotational excitation, we neglect possible effects of Coriolis coupling and compare these tunneling splittings with the experimentally measured splittings for the $j=1$, $k=1$ state.

To develop dynamical approximations that require only ground state methods, we make use of the fact that three different time scales are involved. The first of these is determined by the van der Waals interaction between the helium atoms and the ammonia molecule. The other two time scales are associated with the internal inversion mode of the ammonia, namely, the fast time scale of the vibrational frequency ν_2 and the slow time scale of the tunneling frequency δ. This suggests two different approximations that are both based on the separation of each of these two aspects of the umbrella mode from the van der Waals modes. The first approximation (I) consists of averaging the $He-NH_3$ potential over the eigenfunctions of the umbrella mode of NH_3 in the gas phase to construct a vibrational state dependent $He-NH_3$ potential, which is then used in ground state cluster calculations for each NH_3 vibrational level m. This approximation is justified by the frequency of the inversion mode being much higher than the $He-NH_3$ van der Waals modes and has been used in other calculations of vibrational shifts for molecules in rare gas clusters.[8,9] In the remainder of the paper, we refer to this approximation (I) as vibrationally averaged NH_3, or "fast umbrella vibration, slow helium." The second approximation (II) is an adiabatic approximation in which we compute the ground state energy of a cluster composed of n ^{4}He atoms together with an NH_3 molecule having a fixed geometry. This is characterized by a constant inversion angle of the umbrella mode α defined in the restricted C_3 geometries for NH_3 as the angle between the C_3 axis and the three equivalent NH bonds.[19] Thus, $\alpha=\pi/2$ corresponds to planarity. The α-dependent energies obtained are then used as an extra potential term for the one-dimensional umbrella mode inversion problem. The use of this second, adiabatic approximation here was motivated by two features of the NH_3 inversion in helium. First, the effective mass for the NH_3 inversion mode is quite close to the mass of helium [2.49 amu (Ref. 25) relative to 4.00 amu for ^{4}He]. Second, the tunneling splitting values in the NH_3 double well, in the absence of helium, are of the same order of magnitude as the van der Waals modes [0.8 cm^{-1} (Ref. 26) relative to a few wavenumbers for collective modes of helium droplets[27]]. We refer to this approximation (II) as adiabatic helium response to NH_3 inversion, or "slow umbrella tunneling, fast helium." Within this second approximation, we undertake two types of calculations, namely, with and without the rotational kinetic energy operator of the ammonia molecule.

Each of these two different approximations can be justified by taking one aspect of the NH_3 intramolecular dynamics to be dominant. The use of these two very different approximations and comparison with exact methods therefore allow us to explore what are the critical time scales in this situation. We therefore compare these approximations with results obtained from POITSE for selected cluster sizes.

In this work, we characterize the NH_3He_n system by $3n$ Cartesian coordinates of the n helium atoms in a space fixed frame, the three Cartesian coordinates of the center of mass of the ammonia molecule, the inversion coordinate for NH_3, and, when the rotation is included, by the three Euler angles giving the orientation of the principal axis frame of NH_3 with respect to the space fixed frame. The corresponding Hamiltonian is given by

$$\hat{H} = -\frac{\hbar^2}{2m_{\mathrm{He}}}\sum_{i=1}^{n}\nabla_i^2 - \frac{\hbar^2}{2M}\nabla_{\mathrm{NH_3}}^2 - \frac{\hbar^2}{2\mu}\frac{\partial^2}{\partial h^2} - B_x(h)\frac{\partial^2}{\partial \varphi_x^2} - B_y(h)\frac{\partial^2}{\partial \varphi_y^2} - B_z(h)\frac{\partial^2}{\partial \varphi_z^2} + \sum_{i<j}^{n} V^{\mathrm{HeHe}}(r_{ij}) + \sum_{i=1}^{n} V^{\mathrm{NH_3He}}(\alpha[h], R_i, \theta_i, \phi_i) + V^{\mathrm{1D}}(h), \tag{4}$$

where φ_x, φ_y, and φ_z correspond to a rotation around the x, y, and z principal axes of NH_3, h is the inversion coordinate, m_{He} is the mass of ^{4}He, M is the mass of NH_3, and $B_x(h)$, $B_y(h)$, and $B_z(h)$ are the rotational constants of NH_3. Note that the rotational operators, written here in the principal axis frame of the molecule, are implicitly also dependent on the Euler angles of the NH_3 molecular, describing the molecule orientation in the space fixed frame. Expressing the rotational operators in the principal axis frame is the natural form for developing a short time approximation to the rotational Green's function, the central ingredient for implementation of a rigid body diffusion Monte Carlo scheme.[28] The interaction potential is taken to be the sum of pairwise terms for the He–He and the NH_3-He interactions. For $V^{\mathrm{HeHe}}(r_{ij})$, we use the empirical potential of Aziz *et al.*[29] The NH_3-He interaction potential $V^{\mathrm{NH_3He}}$ is a function of the umbrella inversion angle α and of the position R, θ, ϕ of the helium atom in a frame attached to the molecule.[19] Geometry considerations show that the angular inversion coordinate α used in the potential $V^{\mathrm{NH_3He}}$ is directly related to the inversion coordinate h, which is the distance between N and the H_3 plane that is used in the one-dimensional Hamiltonian representing the umbrella mode. To relate h to α, we use the form

$$\alpha = \gamma_0 + \gamma_1 h + \gamma_3 h^3 + \gamma_5 h^5. \tag{5}$$

The N–H distances have been previously optimized for 11 α values in the construction of the NH_3-He interaction potential[19] and are summarized in Table I. These are used to calculate the corresponding h values for each α, also shown in Table I. The data set $\{\alpha_i, h_i\}$ is then fitted to the above form to obtain the parameters γ_0, γ_1, γ_3, and γ_5. The resulting fit parameters for the inversion angle dependence on h are given in Table II.

Due to the h-dependence of the rotational constants in Eq. (4), the full NH_3He_n Hamiltonian contains coupling between the kinetic and potential energy terms. This can readily be dealt with when the dependence on h is only parametric. This is the situation in approximation (II) below, for which the helium motion is fast relative to the umbrella tun-

TABLE I. Correspondence between the umbrella angle α (in deg) and the distance h (in a.u.) taking into account the change of the distance R_{H-N} (in a.u.).

α	90	95	100	105	110	115	120	125	130	135	140
R_{H-N}	1.872	1.874	1.879	1.887	1.897	1.909	1.924	1.943	1.966	1.996	2.038
h	0.000	0.163	0.326	0.488	0.649	0.807	0.962	1.114	1.264	1.411	1.561

neling. For this case, we compare the results of calculations made with the full h-dependence (or equivalently, the α-dependence) of the rotational constants, with calculations made using averaged values (Sec. III). We find that the results are independent of the h-dependence of the rotational constants, which is understandable, given the small magnitude of the rotational kinetic energy relative to the potential energy. This justifies neglect of the h-dependence also in the full dimensional calculations and in approximation (I) where the helium motion is slow relative to the umbrella tunneling. In these cases, h-dependent B values would modify the effective masses of the rotational kinetic energy terms during a diffusion Monte Carlo propagation, affecting the detailed balance conditions, in addition to introducing errors due to noncommutation of kinetic and potential terms.

1. Approximation (I): Fast umbrella vibration, slow helium

In this first approximation, (I), we make use of the fact that the inversion mode is much faster than the helium motion and also neglect the h-dependence of the rotational constants shown in Eq. (4). Thus, we first solve the one-dimensional Hamiltonian

$$\hat{H}_{\mathrm{I}}^{1\mathrm{D}} = -\frac{\hbar^2}{2\mu}\frac{\partial^2}{\partial h^2} + V^{1\mathrm{D}}(h), \tag{6}$$

which represents the umbrella mode of the gas phase NH_3 species. We then construct vibrationally averaged NH_3–He potentials by averaging over vibrational eigenfunctions $|\psi_m\rangle$ of this umbrella mode:

$$V_{\mathrm{I}}(m) = \sum_{i<j}^{n} V^{\mathrm{HeHe}}(r_{ij}) + \sum_{i=1}^{n} \langle \psi_m | V^{\mathrm{NH_3He}}(\alpha, R_i, \theta_i, \phi_i) | \psi_m \rangle_\alpha. \tag{7}$$

The notation $\langle\ \rangle_\alpha$ indicates integration over α, which is equivalent to integration over h. For $|\psi_m\rangle$, we employ here the vibrational eigenfunctions of gas phase NH_3 (see Sec. II A 3), consistent with previous constructions of vibrationally averaged potentials for molecules in helium.[8] The integration over α in Eq. (7) is done numerically using a DVR representation of the eigenfunctions $|\psi_m\rangle$.[30,31] Details are given in Sec. II A 3 below.

These vibrationally averaged potentials are then used in ground state diffusion Monte Carlo calculations with the m-dependent cluster Hamiltonian

TABLE II. Fit parameters for Eq. (5) (α in deg, h in a.u.).

γ_0	γ_1	γ_3	γ_5
90	30.46	0.912	–0.106

$$\hat{H}_{\mathrm{I}} = -\frac{\hbar^2}{2m_{\mathrm{He}}}\sum_{i=1}^{n}\nabla_i^2 - \frac{\hbar^2}{2M}\nabla_{\mathrm{NH_3}}^2 - B_x\frac{\partial^2}{\partial\varphi_x^2} - B_y\frac{\partial^2}{\partial\varphi_y^2} - B_z\frac{\partial^2}{\partial\varphi_z^2} + V_{\mathrm{I}}(m), \tag{8}$$

for each m level of interest. This approximation corresponds to the umbrella mode being treated as fast relative to the helium modes, i.e., it is based on a separation of time scales of the fast inversion vibrational dynamics from the slow van der Waals dynamics. Under these conditions, the ground states E_m obtained with energy levels $m=1-4$ correspond to the ground and first three excited states of the umbrella mode in the presence of the helium cluster. We can then estimate the vibrational shift $\delta\nu_2$ from Eq. (1) after subtracting the gas phase frequency ν_2 from the energies E_m, and can calculate the effective tunneling splittings $\tilde{\delta}_0/\delta_0$ and $\tilde{\delta}_1/\delta_1$ from Eqs. (2) and (3).

Since in approximation (I) the helium atoms move on an inversion-averaged potential surface, they effectively feel an averaged molecular structure of the NH_3 molecule. In principle, this averaged molecular structure and hence the rotational constants should dependent on the vibrational state $|\Psi_m\rangle$ via the h-dependence of B_x, B_y, and B_z. However, in order to perform correlated sampling (Sec. II B 1), it is necessary to use a single set of rotational constants, since the rotational kinetic energy influences the sampling of the random walk over which multiple potential terms are evaluated. We therefore use the vibrational ground state rotational constants in these calculations using the experimental values $B_x=B_y=9.96\ \mathrm{cm}^{-1}$ and $B_z=6.2\ \mathrm{cm}^{-1}$.[16,17,26] Results obtained with this first approximation are described in Sec. III C.

2. Approximation (II): Slow umbrella tunneling, fast helium

The second approximation, (II), is an adiabatic approximation in which the geometry of the NH_3 molecule is first fixed at a specific value of α and a ground state calculation of the molecule-helium cluster made with the Hamiltonian

$$\hat{H}_{\mathrm{II}} = -\frac{\hbar^2}{2m_{\mathrm{He}}}\sum_{i=1}^{n}\nabla_i^2 - \frac{\hbar^2}{2M}\nabla_{\mathrm{NH_3}}^2 - B_x(h)\frac{\partial^2}{\partial\varphi_x^2} - B_y(h)\frac{\partial^2}{\partial\varphi_y^2} - B_z(h)\frac{\partial^2}{\partial\varphi_z^2} + \sum_{i<j}^{n} V^{\mathrm{HeHe}}(r_{ij}) + \sum_{i=1}^{n} V^{\mathrm{NH_3He}}(\alpha, R_i, \theta_i, \phi_i) \tag{9}$$

to obtain a cluster energy $E[h(\alpha)]$. The interaction potential for this approximation is thus given by

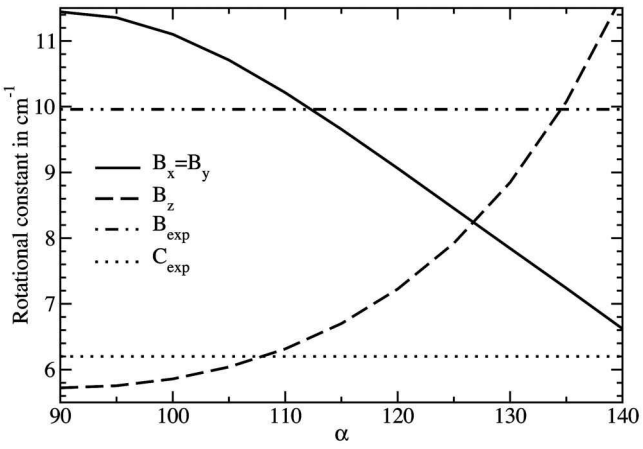

FIG. 1. Dependence of the three rotational constants of NH_3 (in cm^{-1}) on the umbrella angle α (in deg), shown together with the experimental gas phase average values $B_{exp}=9.96\ cm^{-1}$ and $C_{exp}=6.2\ cm^{-1}$ (Ref. 16, 17, and 26).

$$V_{II}(\alpha[h]) = \sum_{i<j}^{n} V^{HeHe}(r_{ij}) + \sum_{i=1}^{n} V^{NH_3He}(\alpha, R_i, \theta_i, \phi_i), \quad (10)$$

in which the umbrella angle α (or equivalently, the inversion coordinate h) is a parameter. The value of the cluster energy relative to the corresponding value for the planar geometry, $E[h(\alpha=90°)]$, defines the perturbation on the NH_3 inversion coordinate that is induced by the helium cluster. These $h(\alpha)$-dependent cluster energies are computed over the entire range of $h(\alpha)$, and the energy $W(h)=E[h(\alpha)]-E[(\alpha=90°)]$ is then added to the remaining h-dependent terms in Eq. (4) to yield an effective one-dimensional inversion Hamiltonian

$$\hat{H}^{1D} = -\frac{\hbar^2}{2\mu}\frac{\partial^2}{\partial h^2} + V^{1D}(h) + W(h). \quad (11)$$

This one-dimensional inversion Hamiltonian is then solved to yield the total energies. The first four eigenvalues correspond to the energy levels E_i, $i=1-4$ of Eqs. (1)–(3). This second adiabatic approximation therefore corresponds to the umbrella mode being treated as slow and the helium atoms as fast, i.e., it is based on an adiabatic separation of the intramolecular tunneling dynamics from the van der Waals dynamics.

In this second approximation, we are able to compute the moment of inertia and hence the rotational constants for the actual NH_3 geometry resulting at each value of α, yielding $B(\alpha)$. By the analysis given above (see Table I), this is equivalent to the function $B(h)$ used in Eq. (4). The α-dependence of the three rotational constants is shown in Fig. 1, where they are also compared with the experimentally measured values. We see here that as α increases, the NH_3 molecule goes from an oblate symmetric top ($B_x=B_y>B_z$, i.e., $A=B>C$) to a prolate one ($B_z>B_x=B_y$, i.e., $A>B=C$). The experimentally determined gas phase structure corresponds to a slightly oblate symmetric top, with $\alpha\sim110°$.[26] The experimental values correspond to B values averaged over the vibrational ground state. While it would be possible, in principle, to average over the ground state vibrational wave function to obtain vibrationally averaged rotational constants to compare with the experimental values, accurate determination of the full dimensional vibrational ground state is not trivial. We use the experimental values $B_x=B_y=9.96\ cm^{-1}$ and $B_z=6.2\ cm^{-1}$ for the calculations with helium in this second approximation after having tested the sensitivity of the results to the geometry-dependent changes in B_x, B_y, and B_z for NH_3He. For the smallest cluster size, we compared the results obtained using the experimental averaged rotational constants to the one using the α-dependent rotational constants. We have also tested the effect of the molecular rotation itself by artificially suppressing the corresponding kinetic part in the Hamiltonian ($B_x=B_y=B_z=0$). These tests are described in Sec. III D.

3. Inversion levels of NH_3

In both approximations, the inversion levels have to be characterized. The Schrödinger equation of the inversion mode is a one-dimensional differential equation which can be trivially solved by means of a basis set expansion. The general Hamiltonian is given by Eq. (11), with h the distance between N and the H_3 plane, μ the effective mass for this particular mode,[25] V^{1D} the unperturbed double well potential, and $W(h)$ the perturbation due to interaction with the helium atoms. In the first approximation, (I), we set $W(h)=0$, while for the second approximation, (II), the perturbation is given by $W(h)=E[h(\alpha)]-E[\alpha=90°]$, where $E[h(\alpha)]$ are diffusion Monte Carlo (DMC) ground state energies for the cluster with fixed α values.

The one-dimensional (1D) Schrödinger equation for the inversion mode is solved here with the collocation method[30,31] using sine functions as a finite basis representation for which the kinetic term is diagonal:

$$\langle h|S_n\rangle = \sqrt{\frac{1}{2h_{max}}}\sin\frac{n\pi(h+h_{max})}{2h_{max}}, \quad (12)$$

with $n=1,\ldots,151$ and $h_{max}=1.7$ a.u. The number of equidistant grid points in h used for the evaluation of the potential terms is taken to be larger ($N_{DVR}=181$) than the number of sine functions, ensuring the accuracy of the quadrature in the collocation scheme. With this size of basis set, the energy and the wave function of the four first levels are fully converged to an accuracy better than the number of digits reported in this paper.

Approximation (I) requires computation of the effective potential [Eq. (7)] at each time step during the Monte Carlo simulation. The integration over the DVR points in Eq. (7) is much more time consuming than the evaluation of the potential term alone. In order to compute the blueshift and the tunneling splitting, four different calculations have to be made, one for each of the four eigenfunctions $|\Psi_m\rangle$. Some of the energy differences between these four systems are very small, compared to the actual energy of the level, and, consequently, it is essential to use correlated sampling in evaluating the energy differences.[32,33] The CPU time can also be optimized here by noting that the four integrations over α are similar, i.e.,

$$\langle \Psi_m | V^{NH_3He}(\alpha,R,\theta,\varphi) | \Psi_m \rangle_\alpha = \sum_{p=1}^{N_{DVR}} c_{mp} c_{mp}^* V^{NH_3He}(\alpha_p,R,\theta,\varphi), \quad (13)$$

where c_{mp} is the DVR coefficient of the mth level on the pth grid point in α. The effective potentials for the four $|\Psi_m\rangle$ functions differ from one another only in the c_{mp} coefficients. They can thus be computed within a correlated sampling scheme using only N_{DVR} calls of the NH_3–He potential. The ground state wave function $|\Psi_1\rangle$ is taken to be the model system for the correlated sampling, and the remaining three levels are treated as differential systems.[32] We are thereby able to compute the energy differences $\delta_0=E_2-E_1$, $\delta_1=E_4-E_3$, and $\nu_2=[(E_4-E_2)+(E_3-E_1)]/2$ with a low variance.

For the adiabatic approximation, (II), the DMC calculations were performed for the 11 fixed values of α that are used for the creation of the ammonia-helium potential in Ref. 19 ($90° \leqslant \alpha \leqslant 140°$). In order to have an analytical expression for $E[h]$ and thus for $W(h)$, we fit the energies to the following polynomial expression:

$$E[h]^{fit} = E[\alpha = 90°] + c_2 h^2 + c_4 h^4 + c_6 h^6 + c_8 h^8, \quad (14)$$

for each cluster size. In this approximation, the decoupling of the inversion mode from the other degrees of freedom also allows us to easily use different effective one-dimensional potentials for the inversion mode, i.e., for the unperturbed double well potential V^{1D}, and to check the effect of these on the computed shifts. For this purpose, we have tested two of the expressions for V^{1D} given in Ref. 25, which we denote as V_b^{1D} and V_f^{1D} (corresponding to V_b and V_f, respectively, of Ref. 25). The potential form V_f^{1D} and its associated mass μ were optimized by Niño and Muñoz-Caro in Ref. 25 to reproduce the observed spectral lines in gas phase NH_3. However, single point quantum chemistry energy calculations[34] made at the CCSD(T)/aug-cc-pVQZ level for the same geometries that were used for the creation of V^{NH_3He} in Ref. 19 are in agreement with V_b^{1D} rather than with V_f^{1D}. We have therefore used V_b^{1D} for time consuming computations, like the first approximation or the POITSE calculation (see below), since this ensures a fully consistent potential. Moreover, it is reasonable to assume that the effect of the choice of the one-dimensional inversion potential should be small on quantities such as the ratio of the tunneling splitting observed in helium cluster and the one for the free molecule, i.e., $\tilde{\delta}/\delta$. We verify this explicitly by comparison of selected results obtained with both V_b^{1D} and V_f^{1D}.

4. Beyond approximations based on separation of time scales: POITSE calculations

In order to perform calculations beyond the two approximations presented before, we consider simultaneously the translational motion of all particles of the system (n helium atoms and NH_3), the rotation of the NH_3 molecule, and its inversion. In these calculations, the full Hamiltonian [Eq. (4)] is used directly, resulting in $3n+7$ degrees of freedom. The computation of excited states is done using the POITSE method.[22,35] We have chosen to use the experimental value for the rotational constants $B_x=B_y=9.96\ cm^{-1}$ and $B_z=6.2\ cm^{-1}$ (Refs. 16, 17, and 26) here since the comparative studies made within the adiabatic approximation (II) presented in Sec. III D were found to show only a small sensitivity of the results to the geometry-dependent changes in B. This also facilitates the comparison with approximation (I), for which the same experimental values for B_x, B_y, and B_z were used (see above).

B. Monte Carlo techniques

1. Diffusion Monte Carlo

In the present study, we use several variants of the diffusion Monte Carlo (DMC) method to evaluate vibrational shifts and intramolecular tunneling splittings of the NH_3 molecule inside ^4He_N, for $1 \leqslant N \leqslant 40$. Since DMC methodologies have already been described in numerous publications,[28,36–40] we provide here only the main features of the method and some details specific to its current application to NH_3He_n.

In DMC with importance sampling, the working equation for a $\mathcal{N}$-dimensional system can be written as[36]

$$\frac{\partial f(\mathcal{X})}{\partial \tau} = \sum_j^{\mathcal{N}} \{D_j \nabla_j^2 f(\mathcal{X}) - D_j \nabla_j [f(\mathcal{X}) F_j(\mathcal{X})]\} - [E_l(\mathcal{X}) - E_{ref}] f(\mathcal{X}), \quad (15)$$

where $\mathcal{X}$ is a vector in the $\mathcal{N}$-dimensional space, $D_j=\hbar^2/2m_j$ if the jth degree of freedom corresponds to a translation, and $D_j=B_j=\hbar^2/2I_j$ if this degree of freedom corresponds to a rotation. In the above equation, $E_l(\mathcal{X})=\Psi_T(\mathcal{X})^{-1}\hat{H}\Psi_T(\mathcal{X})$ is the local energy and $F_j(\mathcal{X})=\nabla_j \ln|\Psi_T(\mathcal{X})|^2$ is the quantum force. The use of a guiding function is usually referred to as importance sampling DMC or biased DMC, since it improves the sampling of relevant parts of the configuration space where the trial function is large. We use the rigid body DMC scheme to sample the rotational degrees of freedom,[38] taking care to eliminate all time step biases including possible bias due to noncommutation of the rotational degrees of freedom. Explicit detail examples of time step studies are given in Sec. III. Alternative sampling schemes include the SHAKE algorithm.[41]

A random walk technique is used to determine the steady state of Eq. (15). A walker (or configuration) is defined as a vector in the $\mathcal{N}$-dimensional space. It represents the position and orientation of all the particles of the system under study. An ensemble of walkers is propagated from some arbitrary initial distribution using the short time approximation of the Green's function. The statistical representation of this Green's function is made in a two step procedure. First, each coordinate of the walkers is moved according to the sum of a Gaussian distributed random number having a width $\sqrt{2D_j\delta\tau}$ and the quantum drift force $D_j\delta\tau F_j(\mathcal{X})$. The statistical representation of the potential dependent factor in the Green's function can be made using at least three different schemes. In one scheme, this factor is implemented through a branching scheme in which walkers can be either kept, destroyed, or replicated. However, this scheme has the disadvantage that the ensemble size is not necessarily constant during the

propagation. A second scheme uses continuous weights. Here, each walker carries a weight $\mathcal{W}_i$, which is updated at every time step according to

$$\mathcal{W}_i(\tau+\delta\tau)=\mathcal{W}_i(\tau)\exp\left(E_{\mathrm{ref}}-\frac{E_l(\mathcal{R})+E_l(\mathcal{R}')}{2}\right). \quad (16)$$

While the scheme with continuous weights is more attractive, it is not stable numerically. This is because after even a moderate propagation time, the distribution of weights among the walkers is no longer uniform, with very few walkers sometimes carrying extremely large weights. In fact, the divergence of this scheme has been proven rigorously.[42] It can be overcome by using a combination of weights and branching.[9] When doing this, particular care must be taken to avoid a systematic effect of branching on the sum of weights. The scheme we use here is a fixed ensemble size approach similar to that of Lewerenz which was employed in Ref. 9. Its implementation is also described in Ref. 43. The scheme works by first looking for walkers with low weights. If the relative weight $\mathcal{W}_i^{\mathrm{rel}}(\tau)=\mathcal{W}_i(\tau)/\Sigma_i\mathcal{W}_i(\tau)$ of a walker becomes lower than $\mathcal{W}_{\mathrm{min}}$ (we choose $\mathcal{W}_{\mathrm{min}}=0.5$ in these studies), an attempt to kill is made with a probability $1-\mathcal{W}_i^{\mathrm{rel}}(\tau)$. If the walker is killed, in order to conserve ensemble size, then we take the walker (j) with the highest weight and split this into two walkers, each of which carried the weight $\mathcal{W}_j(\tau)/2$. If the walker is not killed, then its weight is reset to the average weight of the ensemble. This treatment of the small and high weights appears to be stable. The loss of weight occurring when small weight walkers are destroyed is on average compensated by the increase of weights when they are artificially reset to the average ensemble weight. The frequency of branching has to be optimized for each system, i.e., for each cluster size. It must be frequent enough to ensure a homogeneous distribution of weights among the walkers, but at the same time, it must be infrequent enough to avoid introducing any bias.

The energy of the system can be computed as the average of either the local energy or the growth energy. The difference between these two estimates gives an indication of the actual time step error introduced both by the trial wave function (usually linear) and by the statistical representation of the Green's function $[\mathcal{O}(\delta\tau^2)$ for $\Psi_T=1]$.[33] In this work, we report the average of the local energy. We have confirmed agreement of this with the average of the growth energy in all cases. As with any stochastic procedure, the Monte Carlo results are subject to a statistical noise and a variance associated with the use of random numbers and finite ensemble sizes. We report as our error estimate here the variance $\sqrt{\langle E\rangle^2-\langle E^2\rangle}$ divided by $\sqrt{N_{\mathrm{block}}}$, where we have split the time evolution into blocks and computed the average using one energy value per block. In order to avoid correlation between successive data values, we checked that the size of the block used was longer than the correlation length.[40]

Even if, in principle, the statistical error can be reduced by increasing the amount of sampling, it can still be larger than the energy difference we are studying. This is particularly relevant to calculation of the tunneling splittings in vibrational states. To overcome this problem, we have made use of the correlated sampling technique in which two or more different systems are sampled at the same time.[32,33] The correlation introduced between these different systems reduces the statistical noise for the energy difference. In the case of the first approximation (I) studied here, we are constructing differential systems that differ from the model system only in the potential energy term in their Hamiltonians [see Eq. (13) for the definition of the four potential energy terms]. This is the classic differential situation studied by Wells.[32] However, we found that a procedure based on pure branching as described in Ref. 32 did not lead to stable results for this NH_3-helium system. This derives primarily from the fact that some walkers destroyed according to the model system are nevertheless still relevant for the differential systems. We therefore modified the procedure of Wells to use a combination of weights and branching. Each walker carries a weight $\mathcal{W}_i^\zeta$ for each of the ζ systems. Each weight $\mathcal{W}_i^\zeta$ is updated at every time step according to

$$\mathcal{W}_i^\zeta(\tau+\delta\tau)=\mathcal{W}_i^\zeta(\tau)\exp\left(E_{\mathrm{ref}}^\zeta-\frac{E_l^\zeta(\mathcal{X})+E_l^\zeta(\mathcal{X}')}{2}\right). \quad (17)$$

Note that this is Eq. (16), adapted to each system ζ. The procedure described above to take care of low and high weights was slightly modified here in order to make sure that no walker still relevant for the representation of any of the systems (model or differential) was destroyed. The model system is denoted as $\zeta=1$ in the following. If the weights of a walker are all below $\mathcal{W}_{\mathrm{min}}$, then the walker is killed with the probability $1-\mathcal{W}_i^1(\tau)$. If the walker is not killed, then all its weights are increased to the average weights of the ensemble for each system ζ. This scheme ensures that all relevant walkers are retained and also that the description of the model system is very similar to the uncorrelated case.

2. POITSE

The POITSE scheme has been shown[23] to overcome the constraint on the nodal surface present in the fixed node approximation. In this scheme, one extracts excited state energies from the two-sided inverse Laplace transform of an imaginary time correlation function $\tilde{\kappa}(\tau)$. The time dependent decay of this correlation function is computed using a multi-dimensional Monte Carlo integration, combined with zero temperature diffusion Monte Carlo sidewalks.[22] The decay of the correlation $\tilde{\kappa}(\tau)$ contains information about energy differences E_f-E_0, where E_0 is the ground state energy and E_f an excited state energy level. The renormalized POITSE correlation function can be written[22] in a convenient form for Monte Carlo evaluation as

TABLE III. Parameter values used for the He-He and He–NH_3 trial wave functions in a.u.

	Φ^{HeHe}	$\Phi^{\mathrm{NH_3He}}$
a	0.0056	0.3
c	3000	12 000

$$\tilde{\kappa}(\tau)=\left[\frac{\langle\tilde{\Psi}_T|A\ \exp[-(\hat{H}-E_0)\tau]A^{\dagger}|\tilde{\Psi}_T\rangle}{\langle\tilde{\Psi}_T|\tilde{\Psi}_T\rangle}\right]\Bigg/\left[\frac{\langle\tilde{\Psi}_T|\exp[-(\hat{H}-E_0)\tau]|\tilde{\Psi}_T\rangle}{\langle\tilde{\Psi}_T|\tilde{\Psi}_T\rangle}\right]. \tag{18}$$

In this equation, A is a local operator chosen to project from the trial function $|\tilde{\Psi}_T\rangle$ onto some excited state $|\Psi_f\rangle$. An inverse Laplace transform of $\tilde{\kappa}(\tau)$ yields the desired spectral function $\kappa(\omega)$,

$$\kappa(\omega)=\sum_f |\langle\tilde{\Psi}_T|A|\Psi_f\rangle|^2\delta(E_0-E_f+\omega). \tag{19}$$

Within a pure branching formulation, where the number of walkers $N(\tau)$ is not kept constant and is instead a function of τ, $\tilde{\kappa}(\tau)$ is given by[22]

$$\tilde{\kappa}(\tau)=\frac{1}{N(\tau)}\sum_{k=1}^{N(\tau)} A^{\dagger}(\mathcal{X}_{j(k)}^{(0)})A(\mathcal{X}_k^{(\tau)}), \tag{20}$$

where $j(k)$ gives the "ascendant" of the current walker k, i.e., the index of the initial walker at $\tau=0$, from which the walker k at time τ originates via branching. The imaginary time τ is renormalized at each time step by the Metropolis acceptance rate to correct from rejected moves. The initial configuration $\mathcal{X}_k^{(0)}$ is distributed according to $\tilde{\Psi}_T^2$ with a variational Monte Carlo (VMC) outer loop.

C. Trial functions and projectors

We employed a radial trial function for importance sampled DMC, taken to be identical for both approximations (I) and (II), and also for all α values. This function was introduced primarily to avoid the unphysical dissociation of helium atoms, which occurs at larger n values when one uses an unbiased DMC scheme for a weakly bound cluster.[28] The overall trial function was taken as a product over all possible pairs

$$\Psi_T(\mathcal{R})=\prod_{i<j}^{n}\Phi^{\mathrm{HeHe}}(r_{ij})\prod_{i=1}^{n}\Phi^{\mathrm{NH_3He}}(R_i), \tag{21}$$

where r_{ij} is the distance between two helium atoms and R_i the distance between the center of mass of NH_3 and one helium atom. This product expression simplifies the computation of quantum forces and kinetic terms in the local energy during the DMC walk. The CPU time was reduced by choosing an exponential form for both Φ^{HeHe} and $\Phi^{\mathrm{NH_3He}}$:

$$\Phi(x)=\exp\left(-\frac{c}{x^5}-ax\right), \tag{22}$$

with a and c parameters, similar to the values used in Ref. 44, reported in Table III. The strategy for computation of the parameters for the NH_3–He component is described in Sec. III B.

In the POITSE calculations, we modify the trial function by introducing the dependence on h. The trial function $\tilde{\Psi}_T$ is now taken to be the product

$$\tilde{\Psi}_T(\mathcal{R},h)=\Psi_T(\mathcal{R})\Psi_{\mathrm{inv}}(h), \tag{23}$$

where $\Psi_{\mathrm{inv}}(h)$ is an analytical fit of the first eigenstate $|\Psi_1\rangle$ of the inversion double well. The parameters of the expression employed for the fit

$$\Psi_{\mathrm{inv}}(h)=a_1[e^{-b_1(h-h_1)^2}+e^{-b_1(h+h_1)^2}]e^{c_1h^4} \tag{24}$$

are given in Table IV.

The choice of the projection operator needed in the POITSE scheme is directly related to the excitation we are looking at, namely, the excitations in the umbrella mode. Even though simple powers of h could, in principle, allow the computation of the excited levels of the double well representing the inversion mode, it has already been shown that they usually result in non-negligible overlap with higher excited levels.[22] We use here the more efficient projectors defined by the ratio of the eigenfunctions,[35,45]

$$A_m(\mathcal{R},h)=\Psi_m(h)/\tilde{\Psi}_T(\mathcal{R},h),\quad m=2,3,4, \tag{25}$$

where $\Psi_m(h)$ are the excited state eigenfunctions of the double well (see Sec. II A 3). The following analytical expressions were fitted to the DVR-FBR eigenfunctions for the lowest three excited states ($m=2$–4):

$$\Psi_2(h)=e^{b_2(h-h_2)^2}-e^{b_2(h+h_2)^2}, \tag{26a}$$

$$\Psi_3(h)=a_3[(h-f_3)e^{b_3(h-h_3)^2}-(h+f_3)e^{b_3(h+h_3)^2}]+d_3e^{c_3h^4}, \tag{26b}$$

TABLE IV. Parameters (in a.u.) for the trial function and for the three projectors used in the POITSE calculations [cf. Eqs. (24) and (26).]

m	h_m	a_m	b_m	c_m	d_m	f_m
1	1.0055	0.3895	4.6796	−2.1136	⋯	⋯
2	0.681	⋯	−10.886	⋯	⋯	⋯
3	0.674	0.785	−11.072	−0.082	−0.0664	0.580
4	0.720	0.768	−12.025	−1.325	−0.314	0.447

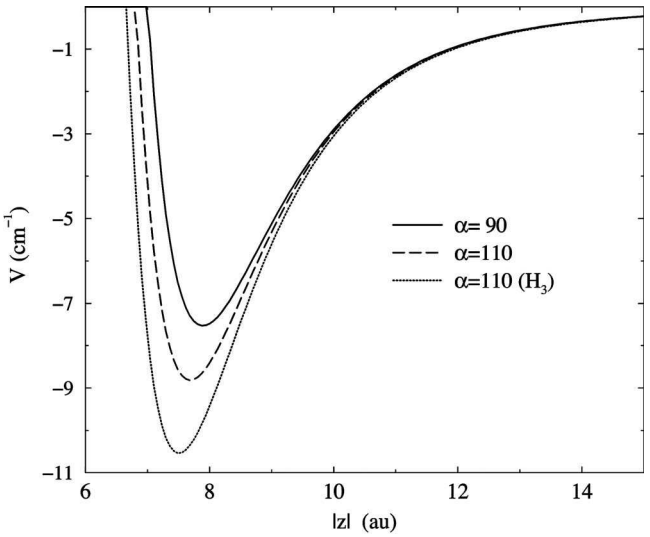

FIG. 2. Cuts (in cm^{-1}) of the potential energy surface along the C_3 axis for $\alpha=90°$ and $\alpha=110°$. The nitrogen atom is at $z=0$, and when the molecule is not planar, the directions pointing toward and away from the H atoms are not identical. For $\alpha=90°$, the potential is identical along z and $-z$. Note that we have represented the cuts as a function of $|z|$ and indicated the direction towards the hydrogen atoms by "H_3."

$$\Psi_4(h) = a_4[(h-f_4)e^{b_4(h-h_4)^2} + (h+f_4)e^{b_4(h+h_4)^2}] + d_4 h e^{c_4 h^4}. \tag{26c}$$

The parameters are given in Table IV.

III. RESULTS

A. Expectations from potential energy surface features

Before undertaking the dynamical calculations, analysis of the potential surface can explain qualitatively why we expect that this potential will induce a reduction of the tunneling splitting and a blueshift for the umbrella mode. This analysis is based on the changes of the He–NH_3 potential surface shape upon inversion of NH_3 and on correlation of this with the one-dimensional eigenfunctions of the umbrella mode. The minimum of the double well potential corresponds to an umbrella angle close to 110°. The planar NH_3 geometry corresponds to the barrier of the double well. The symmetry of the umbrella mode eigenfunctions ensures that the eigenfunctions Ψ_m with even m are exactly zero for the planar geometry, whereas they are nonzero for the states with odd m at the planar geometry. (The ground state is Ψ_1.) Furthermore, the amplitude of the wave function will be higher for the second odd level than for the first one due to a larger tunneling effect in the higher excited state. As seen in Fig. 2, the He–NH_3 potential for the planar NH_3 molecule ($\alpha=90°$) presents a lower attraction along the C_3 axis of NH_3 than for the NH_3 molecule with an α angle of 110°. Thus, energy levels having significant probability amplitude for the planar geometry will be more destabilized than energy levels possessing zero probability for this geometry. This will be the case as soon as enough helium atoms are present and start filling this region of the potential energy surface. The expected behavior of the four first levels can therefore be predicted. The second level will be less destabilized than the first one, inducing a reduction in the first, ground state, tunneling splitting $\delta_0 \rightarrow \tilde{\delta}_0$. The same will occur for the fourth and third levels, which will be responsible for the reduction of the splitting for the vibrationally excited state. A vibrational blueshift is expected since the destabilization of the fourth level is expected to be greater than the corresponding destabilization for the lower level, the amplitude of the wave function being larger for the upper level. Note that for some other positions of the helium atom with respect to NH_3, e.g., for a helium sitting in the plane corresponding to $\alpha=90°$, this argument leads to the opposite conclusion. Nevertheless, when the potential is averaged over all orientations, the same conclusions are obtained as with the above argument given for the helium sitting on the C_3 axis.

This static study is, of course, limited, and dynamical studies have to be performed to confirm these predictions. In the remainder of this section, we first explain the determination of the trial function parameters using a combination of unbiased DMC and the second, adiabatic approximation (II). We then present results for larger clusters obtained within the first approximation (I) using importance sampling. Second, we present the shifts obtained with the adiabatic approximation (II) and compare with those obtained from the vibrationally averaged NH_3 approximation (I). We also show the effect of the rotation of NH_3 and of the choice of the double well potential on the computed vibrational shifts. Lastly, we present the POITSE results that are computed without any dynamical approximation. Here, we take the experimental values $B_x=B_y=9.96\ cm^{-1}$ and $B_z=6.2\ cm^{-1}$ in order to enable a direct comparison with the results from the two approximations we made based on time scale separations (Sec. II).

B. Unbiased DMC, trial wave functions, and time step dependence

In order to define the trial wave function parameters, we performed a systematic study of the radial projection of the effective wave function using unbiased DMC within the second, adiabatic approximation, since this is the least CPU consuming calculation. Since we want to assess the effect of the molecular rotation, we made two kinds of calculation, namely, including or neglecting the NH_3 rotational kinetic energy. In both cases, clusters are less bound for $\alpha=90°$ than for higher α values, even though the well of the interaction potential is deeper for this particular geometry. This is a consequence of the fact that the zero-point energy is a function of α: it is higher at $\alpha=90°$ than at $\alpha>90°$. This reflects the fact that while the potential is deeper at $\alpha=90°$, it is also narrower and this tends to raise the zero-point energy. Furthermore, as pointed out in Ref. 19, the spherically averaged potential is getting broader and other parts of the potential become more significant than the binding energy of the global minimum itself as the molecule moves away from planarity. The unphysical dissociation seen with unbiased DMC when increasing the cluster size[28] is thus occurring sooner at $\alpha=90°$ than at the other ammonia geometries. This dissociation occurs for $n \geqslant 9$ helium atoms and is seen in both the

radial density profiles and the energies. The radial helium density profile at $\alpha=90°$ that is obtained for the largest cluster which is still bound in a unbiased DMC calculation, $NH_3\ ^4He_8$, is used to fit the radial trial wave function parameters. To ensure that the guiding function will include all relevant parts of the configuration space, we further fit with a power of 0.8 instead of using the actual radial profile, thereby obtaining a broader function. This ensures that the relevant configuration space can be adequately sampled and is important to check to avoid unphysically high energies.[28] The corresponding parameter values for both cases of a fixed and rotating NH_3 molecule are given in Table III.

We performed a series of computations varying the time step from 800 a.u. down to 25 a.u. and the number of walker in the ensemble size from 2000 up to 8000 walkers for the clusters NH_3He_n, $n=1,3,8$. The time step dependence of the density profiles was found to be negligible below a time step of 100 a.u. The differences observed between results from calculations with ensemble sizes of 2000 and of 4000 are also insignificant after fitting to the trial function. While the absolute values of the energies do show some dependence on time step and ensemble size, these dependences cancel out when the energy differences in Eqs. (1)–(3) are evaluated. Time step sizes of 50 a.u. are then sufficient to converge the vibrational shifts and tunneling splittings for all calculations within the two approximations described in Secs. III C and III D. The full dimensional POITSE calculations place more stringent requirements on the time step, and smaller values of ~10 a.u. or even below are required to converge these calculations. Detailed time step studies of the excited state energies obtained from the POITSE calculations are presented in Sec. III E.

C. Results from approximation (I): Fast umbrella vibration, slow helium

Here, the helium atoms evolve in a potential that is averaged over the eigenfunctions of the fast vibrational motions of the NH_3 molecule, which, in this case, correspond to the umbrella mode. All calculations include the rotation of NH_3 and use V_b^{1D} for the umbrella mode potential. Since in this approximation the umbrella mode is averaged over one of the one-dimensional umbrella states, the α-dependence of the rotational B values is not meaningful here. As noted in Sec. II, we therefore represent the rotational constants by the experimental values $B_x=B_y=9.96\ cm^{-1}$ and $B_z=6.2\ cm^{-1}$. The lowest umbrella mode energy E_1 is computed directly and the next three levels of interest, and E_2, E_3, and E_4 are computed simultaneously by correlated sampling as described in Sec. II B. We use a time step of 50 a.u. and the radial wave function described in Sec. II. Identical results are obtained with a time step of 100 a.u. The validity of our correlated sampling scheme implementation has been tested on NH_3He_6, for which separate importance sampling computations were performed using the three averaged potentials defined in Eq. (13) for $m=1$, 3, and 4. Computations with $m=2$ have not been attempted since the difference of energy of this state from $m=1$ is extremely small. The corresponding energy differences compare well, with values $E_3-E_1=2.221\pm0.006\ cm^{-1}$ and $E_4-E_1=1.263\pm0.004\ cm^{-1}$ for the correlated scheme and values $E_3-E_1=2.15\pm0.14\ cm^{-1}$ and $E_4-E_1=1.22\pm0.14\ cm^{-1}$ for separate computations. The shift values $\delta\nu_2$ are then obtained from Eq. (1) after subtraction of the NH_3 vibrational frequency $992.95\ cm^{-1}$ (using V_b^{1D} as the inversion double well potential) and the tunneling splittings calculated from Eqs. (2) and (3).

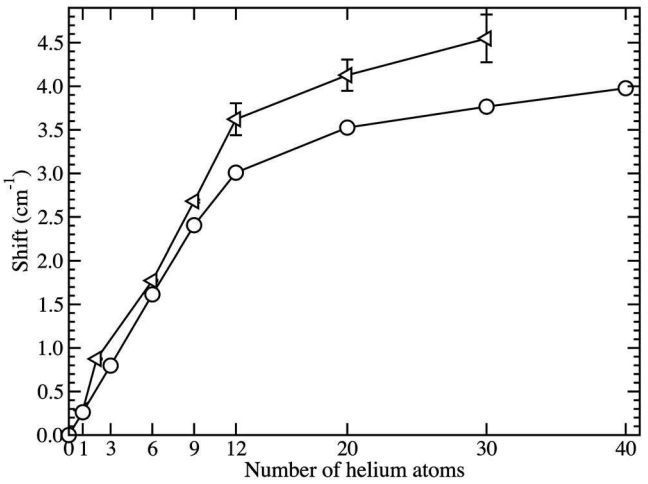

FIG. 3. Evolution of the blueshift of the umbrella mode, $\delta\nu_2$, in cm^{-1} with the cluster size, as calculated from the first approximation (I) with vibrationally averaging over the umbrella mode of NH_3 (open triangles) where this is represented by the double well potential V_b^{1D}. For comparison, we have also shown the values obtained within the second, adiabatic approximation described in Sec. III D using the same double well potential V_b^{1D} and including NH_3 rotation (open circles).

The resulting vibrational shifts are presented in Fig. 3 (open triangles) as a function of the cluster size. For all sizes studied here, we observed a blueshift for ν_2. The value of the shift increases with the number of helium atoms in the cluster. By extrapolating the curve, we expect to see a saturation for approximately 40–50 helium atoms. The extrapolated saturation value is estimated to lie in the range of $4-5\ cm^{-1}$, which is twice the most recent experimental value[17] ($2.1\ cm^{-1}$) and much lower than the earlier estimate[16] ($17.5\ cm^{-1}$).

Figure 4 presents the ratios of the tunneling splittings to their gas phase values, i.e., $\tilde{\delta}_0/\delta_0$ and $\tilde{\delta}_1/\delta_1$, within this first approximation. The two tunneling splittings decrease as the number of helium atoms increases, the decrease for the ground state being larger than the one for the excited state. The ratios obtained for the largest cluster size studied within this approximation ($n=30$) are 96% for the ground state and 97.5% for the excited state. These values are in relatively good agreement with the most recent experimental values of $(101\pm6)\%$ and $(94.4\pm3)\%$ that were extracted in Ref. 17. We note that while the experimental ground state tunneling splitting was found there to be unchanged within the experimental accuracy, the accuracy of the measurements in Ref. 17 was only to ±6%. Most significantly, the theoretical results do not reproduce the larger reductions seen in the earlier experimental values (75% and 31% for the ground and first excited states, respectively).[16]

We did not consider clusters larger than $n=30$ with this vibrationally averaged NH_3 approximation, since as is evident for the vibrational shifts in Fig. 3 and as is shown in the

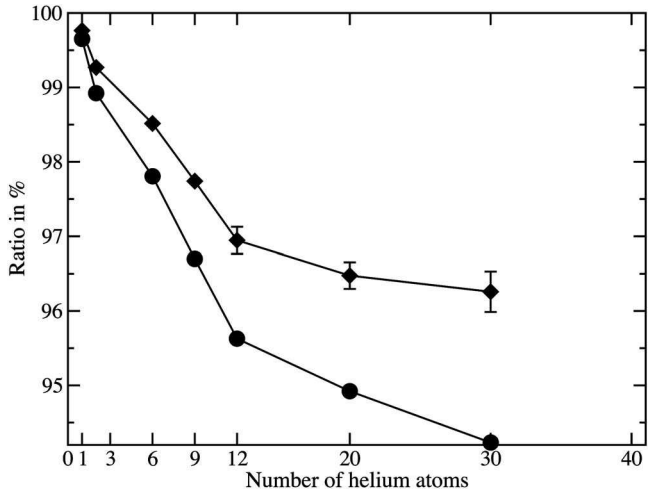

FIG. 4. Evolution of the tunneling splitting ratios $\tilde{\delta}_0/\delta_0$ and $\tilde{\delta}_1/\delta_1$ in % with the cluster size within the first approximation with the double well potential V_b^{1D}. The circles correspond to the ground state and the diamonds to the excited state.

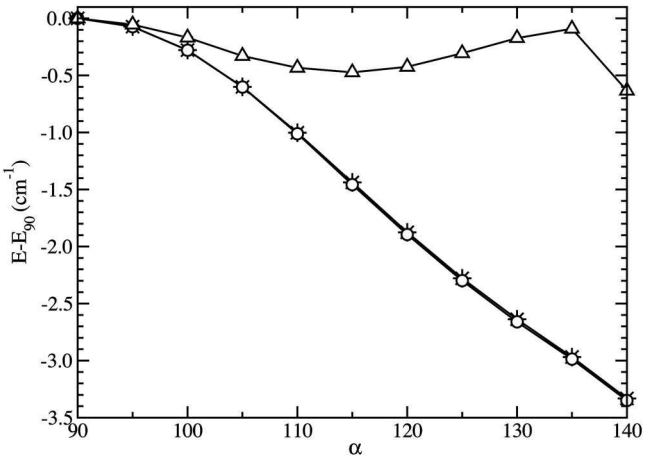

FIG. 5. The energy difference $E[\alpha]-E[90°]$ as a function of α for NH_3 ^4He. The line linking the triangles corresponds to a nonrotating ammonia molecule. The line connecting the open circles corresponds to a rotating molecule with the α-dependent rotational constants, and the line with the asterisks corresponds to a rotating molecule having the experimental B values. Note that the errors bars are smaller than the size of the symbols and that the stars and the open circles are nearly superimposed on this scale.

next section for the tunneling splittings, the results obtained from the two different approximations are very similar, while the second, adiabatic approximation is computationally significantly cheaper to implement.

In summary, within this first dynamic approximation using a vibrationally averaged $He-NH_3$ potential, we are able to reproduce the experimental trend, i.e., a blueshift for the umbrella mode and a reduction of the tunneling splitting, achieving good quantitative agreement with the recent experimental estimates of these.

D. Results from approximation (II): Slow umbrella tunneling, fast helium

In this second approximation, the ammonia molecule is treated as a rigid body with a fixed α angle, corresponding to a fixed value of the inversion coordinate h, and the cluster energy is computed as a function of this coordinate. The cluster energy $W(h)=E[\alpha(h)]-E[\alpha=90°]$ is then employed in the one-dimensional inversion Hamiltonian [Eq. (11)], and the corresponding inversion eigenvalues are computed from which the vibrational shift and tunneling splittings can be calculated as described in Sec. II.

All the cluster calculations were performed using the importance sampling DMC method and the radial trial wave function defined previously. Even if an angular dependence of the guiding function would improve the efficiency of the scheme, it would require optimization of the wave function for each of the α angles. By using the same simple form of radial wave function for all the NH_3 geometries, we are able to deal with clusters having more than nine helium atoms. Moreover, we expect that keeping the same guiding function will cancel out the induced time step error for the $E[h(\alpha)]-E[\alpha=90°]$ computation. For all these calculations, we use a time step of 50 a.u. after having checked that $E[h(\alpha)]-E[\alpha=90°]$ was converged for this value. We check, in particular, the effect of variation of the time step from 25 to 800 a.u. on the quantity $E[\alpha=110°]-E[\alpha=90°]$ for selected cluster sizes. Computation of more α values with a time step of 100 a.u. gives values identical to the results obtained with a time step of 50 a.u.

Figure 5 presents the energy differences obtained for the smallest cluster (NH_3He) in three different calculations. In the first calculation (open triangles), the rotational kinetic energy of NH_3 was neglected, i.e., $B_x=B_y=B_z=0$. In the second calculation (open circles), the rotation was included using the α-dependent B values presented in Fig. 1. In the third calculation (asterisks), the rotation was included using the experimental values of rotational constants, $B_x=B_y=9.96\ cm^{-1}$ and $B_z=6.2\ cm^{-1}$. The rotational kinetic energy of the ammonia molecule has a strong effect on the absolute energy value since the rotational constant of this light molecule is large. We see that the effect of the rotation varies with the actual geometry of the NH_3 molecule, leading to very different $E[\alpha]-E[\alpha=90°]$ curves. For the smallest cluster size, the effect of the choice of the B values, i.e., whether an α-averaged value or the theoretically determined α-dependent values, does not lead to large differences. Using either the α-dependent B values (open circles) or the experimental B values (asterisks) yields very similar energy differences $E[\alpha]-E[\alpha=90°]$. Based on the very small magnitude of the differences observed here, we are therefore justified in employing averaged B values in this adiabatic approximation. With the exception of the smallest values of $\alpha-90°$, the energy difference $E[\alpha]-E[\alpha=90°]$ is significantly larger when the rotational kinetic energy of the molecule is neglected. Furthermore, this curve (triangles) shows a rapid change of slope at $\alpha=140°$. This change of slope is a direct consequence of the change of the location of the global minima in the potential energy surface. For $\alpha=140°$, the helium density is maximum on the C_3 axis, whereas it is maximum on the equatorial plane for the other α values. The regions sampled by the helium atom for $\alpha<140°$ and $\alpha=140°$ are thus very different, resulting in the observed nonmonotonic behavior of the energy dependence on α. Figure 5

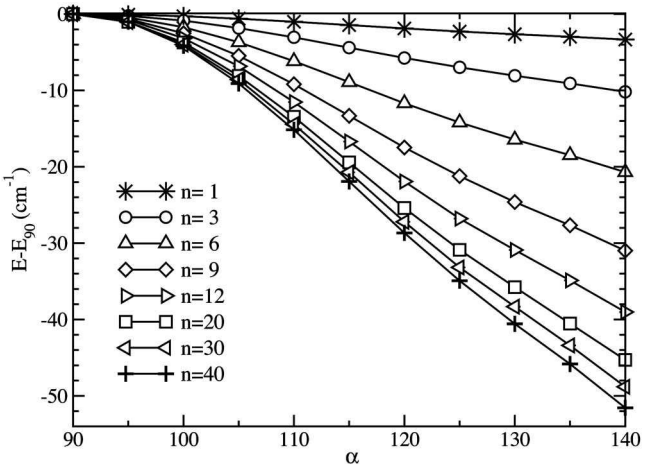

FIG. 6. Evolution of the energy difference $E[\alpha]-E[\alpha=90°]$ as a function of α with cluster size n, computed with a time step of 50 a.u. and 2000 walkers in the ensemble. The error bars are smaller than the size of the symbols. For the smaller clusters, results with a time step of 100 a.u. are not distinguishable on the scale of the figure.

thus shows that while the variation of the geometry-dependent rotational constants about their average values has only a very small effect, neglecting the rotational kinetic term altogether would introduce a significant error into the energies. Thus, the molecular rotational motion is a critical component of the overall energy in this fast helium adiabatic approximation and cannot be neglected.

Figure 6 presents the cluster energy difference $E[\alpha]-E[\alpha=90°]$ for cluster size n varying from 1 to 40. We see that the energy difference saturates for $n \geqslant 30$. Adding the energy differences $W(h)=E[\alpha(h)]-E[\alpha=90°]$ to the inversion potential $V^{1D}(h)$, evaluating the modified one-dimensional energy levels for the inversion degree of freedom, and then subtracting the gas phase vibrational energy yield the vibrational shifts presented in Fig. 7. This plot of $\Delta\nu_2$ versus the number of helium atoms also appears to saturate for $n \geqslant 30$. When using the V_b^{1D} potential, the saturation value is around 4 cm^{-1}, which is again approximately twice

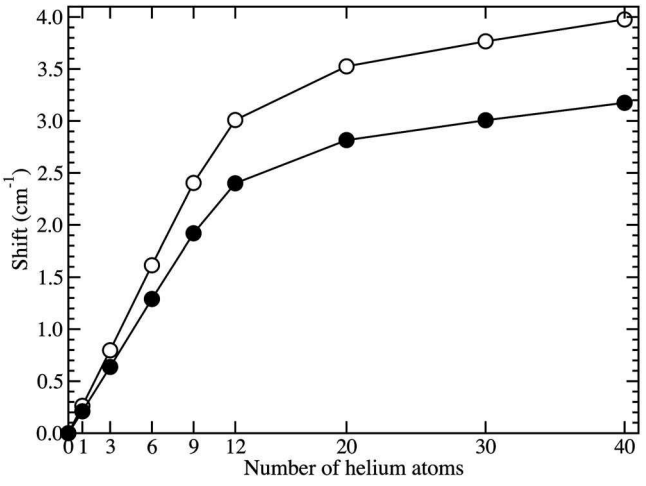

FIG. 7. Evolution of the blueshift (in cm^{-1}) with the cluster size n using the second adiabatic approximation (II). Results obtained with the first double well potential V_b^{1D} are presented as open symbols and results obtained with V_f^{1D} as filled symbols.

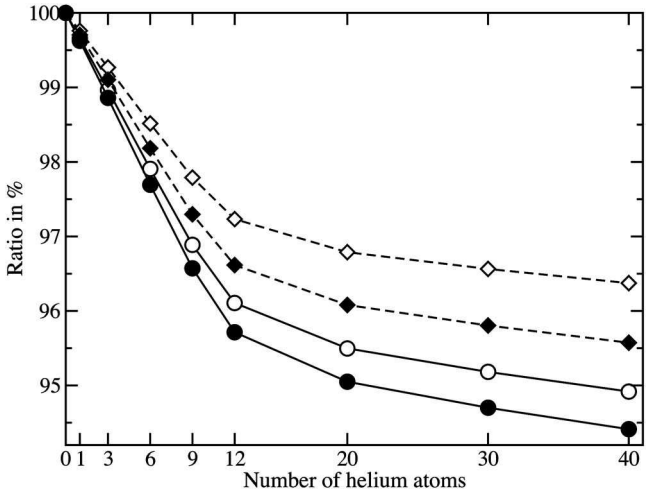

FIG. 8. Evolution of the tunneling splitting ratio $\tilde{\delta}/\delta$, for the ground state (circles) and for the first excited vibrational state (diamonds) with cluster size n, calculated with the second, adiabatic approximation (II). These results were obtained with a rotating NH_3 molecule using both double well potentials V_b^{1D} (open symbols) and V_f^{1D} (filled symbols).

the latest experimental value (2.1 cm^{-1}) and is similar to the results obtained with the vibrationally averaged NH_3 approximation (I) in the previous subsection.

Since in this second, adiabatic approximation (II) the Monte Carlo calculations are independent of the NH_3 internal double well potential, it is straightforward to look at the effect of using different one-dimensional umbrella inversion potentials on the final values of the vibrational shift. In Fig. 7, we therefore also present the results obtained with the second double well potential V_f^{1D}. This has to be used with a different reduced mass, $\mu=2.592\,02$ amu instead of the value $\mu=2.487\,28$ amu used for V_b^{1D}.[25] The computed shifts are seen to be somewhat smaller with V_f^{1D} than with V_b^{1D}, but the behavior of the computed shift is similar in both cases. Since the V_b^{1D} expression agrees with the *ab initio* CCSD(T)/aug-cc-pVQZ energies,[34] we choose to use this latter one-dimensional potential in the following, bearing in mind that our results will be somewhat dependent on this representation of the umbrella mode.

Figure 8 presents the evolution of the tunneling splittings with the cluster size for the rotating NH_3 in the adiabatic approximation (II) using the double well potentials V_b^{1D} and V_f^{1D}, respectively, for the inversion coordinate. The difference between the results obtained from the two inversion potentials is consistent with the differences obtained above. We observe a reduction of both tunneling splittings in the presence of helium. For the larger cluster, the reductions in tunneling splitting values for the ground and excited states are 5% and 3.5% when using the V_b^{1D} potential. These reductions are similar to the most recent experimental values, within the large experimental error bar of ±6%.[17] The value of the ground state tunneling splitting (1.45 cm^{-1} with the potential V_b^{1D}) is much lower than the typical energy range for a molecule-He interaction.[27] Thus, in this case, the second adiabatic approximation appears more appropriate.

Table V summarizes the calculated and experimentally determined vibrational shifts and tunneling splittings. We

TABLE V. Experimental and theoretical (largest helium clusters) vibrational shifts (in cm^{-1}) and tunneling splittings reductions (in %). The results are obtained using the V_b^{1D} potential.

	$\Delta\nu_2$	$\tilde{\delta}_0/\delta_0$	$\tilde{\delta}_1/\delta_1$
Experiment in 1998 (Ref. 16)	17.5	25	68.9
Experiment in 2005 (Ref. 17)	2.1	101	94.4
Adiabatic I (n=30)	4.5	94	96
Adiabatic II (n=40)	4.0	94.9	96.4
POITSE (n=30)		95–96	

find good agreement between the two different approximations tested here. This agreement is significant and indicates that all three motions, the tunneling mode, the helium motions, and the high frequency ν_2 vibrational motion, must therefore be indeed well separated in energy. Our calculations predict a blueshift and a reduction of the tunneling splittings for both the ground and the excited state with a greater percentage reduction in tunneling for the ground state. Comparison with the two available experiments[16,17] shows that our calculations are in better agreement with the more recent one.[17] Our results appear to slightly overestimate the vibrational shift and possibly also the tunneling splittings. However, given the sensitivity of these effects to the inversion potential, a slight overestimation appears quite reasonable. Nevertheless, it is also possible that these approximations based on time scale separations are introducing some systematic error. Therefore, we now go beyond these dynamic approximations by performing POITSE calculations which treat all degrees of freedom on an equal footing.

E. Results from POITSE calculations

In the POITSE calculations, no dynamic approximations are used and all degrees of freedom included here are treated fully quantum mechanically in solving Eq. (4).[22] The power of the POITSE methodology thus lies in its ability to compute excitation energies directly from the ground state, without invoking nodal approximations. The ground state tunneling splitting δ_0 corresponds to such an excitation. The correlation decays obtained with the projector $A_2(\mathcal{R},h)$ defined in Eq. (25) are presented in Fig. 9 for cluster sizes up to 30 helium atoms. The implementation of POITSE was made using the mixed weight and branching scheme described in Sec. II B,[43] time steps of 2.5, 5, and 10 a.u., and an average number of walkers of 2000. Between 3000 and 5000 decays were averaged for each calculation. Since the excitation energy is very small, very long propagation times are needed. After 30 000 a.u., the correlation functions are still above 0.8 for all cluster sizes studied here. For such a restricted portion of the full exponential decay, full inversion using MAXENT (Ref. 22) is not necessary, and a simple linear fitting is adequate as is evident from Fig. 9. The fitted slopes of the decays are then given by $-(E_1-E_0)$ and are a direct measure of the ground state tunneling splitting $\tilde{\delta}_0$. Despite the restricted extent of the exponential decays that we have been able to compute, the correlation functions are clearly seen to decay systematically less rapidly as the number of helium atoms increases. We have found that the decays show some

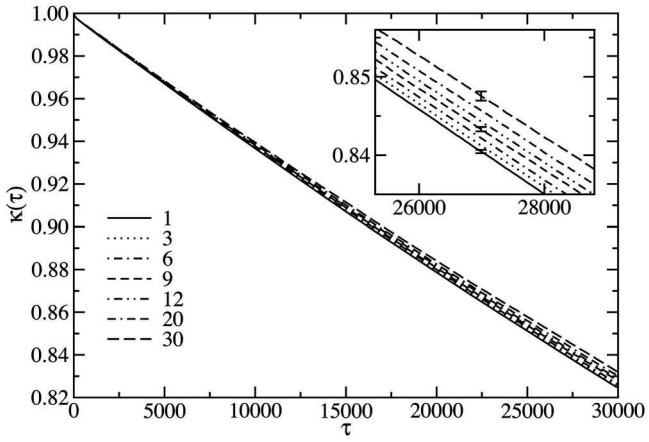

FIG. 9. Renormalized POITSE correlation functions $\tilde{\kappa}(\tau)$ for cluster sizes ranging from n=1 to n=30 helium atoms as a function of imaginary time in a.u. The presented results correspond to an average over 4000–5000 decays using a time step of 2.5 a.u. and an ensemble size of 2000 walkers. A magnification of the later time region is presented in the upper right corner with indication of the error bars for n=1, 9, and 30.

dependence on the time step used in the DMC side walk. However, the ratio of the slopes for different n values are not strongly dependent on the time step and so we can use this to determine the reduction in tunneling splitting relative to that of the n=1 system, as well as to assess the time step dependence in this. In order to do this systematically for decays $\tilde{\kappa}(\tau)$ for different n values, we fit the decay for n=1 and then divide the decay for $n>1$ by this fitted n=1 decay. The short time values of $\kappa(\tau)$ are excluded from the fit since they may contain an admixture of higher excitations. Figure 10 shows the ratios between the decays $\tilde{\kappa}(\tau)$ for different cluster sizes n and the fitted expression of $\tilde{\kappa}(\tau)$ for n=1, at two of the three different time steps studied (2.5 and 10 a.u.). The ratio curves for n=1 are, to a very good approximation, constant and equal to 1, as expected since the normalizing function was derived from the n=1 decay. This confirms that the linear fit used to approximate the correlation decay is accurate. Note that at very small imaginary time values, the ratio is not equal to 1 since the short time decay is excluded from the fit (see above). For larger cluster sizes, the curves presented in Fig. 10 are nearly constant, with values less than 1. The value of this ratio is a measure of the difference in slope of the corresponding correlation decays and is thus also an estimate of the reduction of the tunneling splitting for $n>1$ relative to n=1. Comparison of the left and right panels of Fig. 10, corresponding to time steps of 2.5 and 10 a.u., allows us to conclude that there is negligible effect of time step below 10 a.u.

From Figs. 9 and 10, we extract an estimate of the ground state tunneling excitation using the data calculated with the smallest time step, 2.5 a.u. These evaluations show a reduction of the tunneling splitting for clusters with n helium atoms relative to the value for n=1 that is on the order for 95%–96% for clusters with $n \geqslant 30$. The values extracted for the n=30 cluster are listed in Table V, together with the reductions relative to the gas phase (n=0) values that were calculated with each of the two dynamic approximations (I) and (II), as well as the corresponding experimental value.

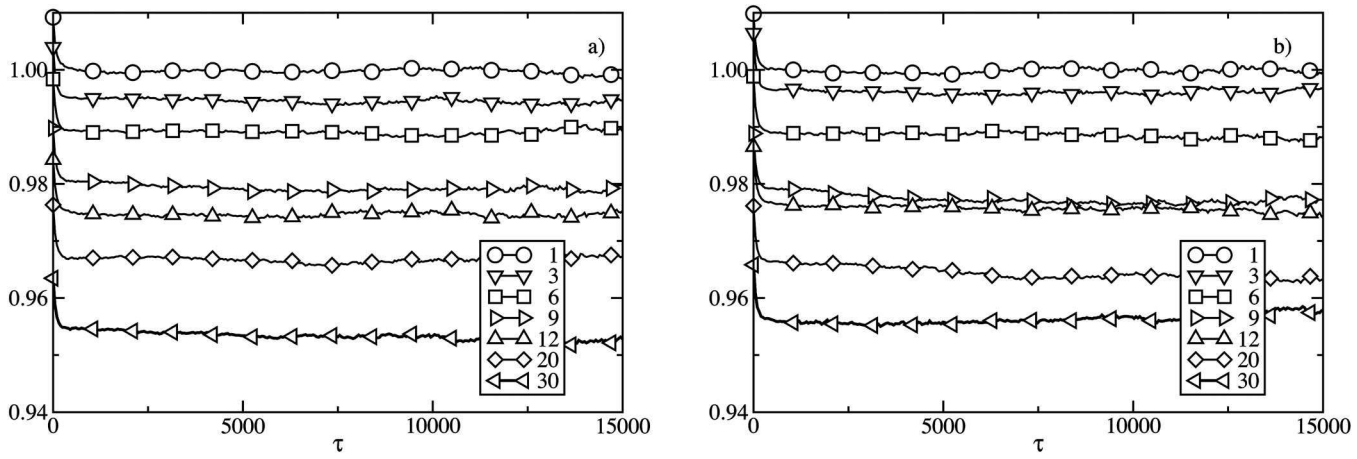

FIG. 10. Variation of the ratio between the correlation decays of Fig. 9 for various n values and of the linear fit of the correlation decay for $n=1$ (i.e., NH_3He) as a function of the imaginary time. The left panel corresponds to computations made with an imaginary time step of 2.5 a.u., while the right panel corresponds to a time step of 10 a.u. Similar results are obtained for the intermediate time step value of 5 a.u.

Since the ground state tunneling splitting reduction that is obtained for $n=1$ from both dynamic approximations is 99.66%, we can take our value for the reduction relative to $n=1$ to be an accurate measure also of the reduction from the $n=0$ gas phase value. The resulting POITSE value for the reduction $\tilde{\delta}_0/\delta_0$ is in good agreement with the recent experimental results of Slipchenko and Vilesov,[17] given the uncertainty of 6% in the latter measurements. It is slightly smaller but quite similar to the values obtained with the two dynamic approximations, and so is also considerably smaller than the earlier experimental reduction of $(25\pm12)\%$ that was claimed in 1998.[16]

Due to computational limitations, POITSE calculations with more than 30 helium atoms have not been performed. Similarly, direct calculation of the tunneling splitting in the excited vibrational state, $\tilde{\delta}_1$, is not practical at the current time since the current implementation of POITSE is restricted to sampling in the ground state. Calculation of an excited state tunneling splitting requires that $\tilde{\delta}_1$ be calculated from the difference of the two large excitation energies E_3-E_1 and E_4-E_1. These excitation energies have error bars that are too large for an accurate determination of the difference.

IV. SUMMARY AND CONCLUSIONS

We have carried out a series of quantum dynamical calculations for the vibrational shift and tunneling splittings of the umbrella mode of NH_3 in helium clusters using an interaction potential that explicitly includes the dependence of the NH_3-He interaction on the umbrella coordinate of NH_3.[19] We employed two different dynamic approximations based on an identification of three disparate time scales, namely, the tunneling motion, the helium dynamics, and the fast umbrella vibrational mode. Both dynamic approximations predicted a blueshift of the umbrella frequency mode and a reduction of the tunneling splittings for both the ground and the first excited states of the umbrella mode in the presence of helium. The saturation values of the vibrational shift and tunneling splittings at $n\sim40$ helium atoms were found to be in good agreement with recent experimental measurements on large helium droplets. The predicted reductions in tunneling splittings were estimated as 5%–6% for the ground vibrational state and as 3%–4% for the first excited vibrational state, while the predicted vibrational shift is of order of $3-5\ cm^{-1}$. While there may be further changes in these quantities as the cluster size is increased to the large droplet regime, the calculated values do appear to approach stationary values for $n\sim30-40$.

As a check on the use of the two dynamic approximations based on time scale separations, the ground state tunneling splittings were also calculated with a full dimensional quantum calculation using the POITSE methodology, which allows a numerically exact calculation without nodal approximations to be made. The POITSE calculations resulted in similar values of reduction of the ground state tunneling splitting to those obtained from the two dynamic approximations, confirming the validity of the time scale separations between the three different dynamical components and the use of either dynamic approximation.

ACKNOWLEDGMENTS

A.V. thanks M. P. Hodges for helpful interactions concerning the use of the potential subroutine as well as discussion of the basic features of the surface. Financial support from the National Science Foundation through NSF Grant No. CHE-0107541 is gratefully acknowledged. We thank the NPACI for computer time at the San Diego Supercomputer center and IDRIS for computer time at the CNRS National Supercomputing Center in Orsay, France. A.V. acknowledges Rennes Metropole for having contributed to the acquisition of a local parallel server.

[1] J. P. Toennies and A. F. Vilesov, Annu. Rev. Phys. Chem. **49**, 1 (1998).
[2] K. B. Whaley, in *Advances in Molecular Vibrations and Collision Dynamics*, edited by J. Bowman and Z. Bačić (Academic, New York/JAI, Greenwich, CT, 1998), Vol. III.
[3] C. Callegari, K. K. Lehmann, R. Schmied, and G. Scoles, J. Chem. Phys. **115**, 10090 (2001).
[4] Y. Kwon, P. Huang, M. V. Patel, D. Blume, and K. B. Whaley, J. Chem. Phys. **113**, 6469 (2000).

[5] J. P. Toennies and A. F. Vilesov, Angew. Chem., Int. Ed. **43**, 2622 (2004).
[6] M. Hartmann, R. E. Miller, A. F. Vilesov, and J. P. Toennies, Phys. Rev. Lett. **75**, 1566 (1995).
[7] R. N. Barnett and K. B. Whaley, J. Chem. Phys. **99**, 9730 (1993).
[8] F. Paesani, F. A. Gianturco, and K. B. Whaley, J. Chem. Phys. **115**, 10225 (2001).
[9] D. Blume, M. Lewerenz, F. Huisken, and M. Kaloudis, J. Chem. Phys. **105**, 8666 (1996).
[10] K. Nauta and R. E. Miller, J. Chem. Phys. **113**, 9466 (2000).
[11] R. Fröchtenicht, M. Kaloudis, M. Koch, and F. Huisken, J. Chem. Phys. **105**, 6128 (1996).
[12] K. Nauta and R. E. Miller, J. Chem. Phys. **113**, 10158 (2000).
[13] M. Behrens, U. Buck, R. Fröchtenicht, M. Hartmann, and M. Havenith, J. Chem. Phys. **107**, 7179 (1997).
[14] A. Sarsa, Z. Bačić, J. W. Moskowitz, and K. E. Schmidt, Phys. Rev. Lett. **88**, 123401 (2002).
[15] H. Jiang, A. Sarsa, G. Murdachaew, K. Szalewicz, and Z. Bačić, J. Chem. Phys. **123**, 224313 (2005).
[16] M. Behrens, U. Buck, R. Fröchtenicht, M. Hartmann, F. Huisken, and F. Rohmund, J. Chem. Phys. **109**, 5914 (1998).
[17] M. N. Slipchenko and A. F. Vilesov, Chem. Phys. Lett. **412**, 176 (2005).
[18] After this paper was completed, we learned of a new experimental microwave study of NH_3 in helium droplets [R. Lehnig, N. V. Blinov, and W. Jager, J. Chem. Phys., preprint, 2007 (submitted)] that shows a similar reduction of 8% in the ground state tunneling splitting relative to its gas phase value.
[19] M. P. Hodges and R. J. Wheatley, J. Chem. Phys. **114**, 8836 (2001).
[20] G. Herzberg, *Molecular Spectra and Molecular Structure II: Infrared and Raman Spectra of Polyatomic Molecules* (Van Nostrand, Princeton, 1966).
[21] E. Lee, D. Farrelly, and K. B. Whaley, Phys. Rev. Lett. **83**, 3812 (1999).
[22] D. Blume, M. Lewerenz, P. Niyaz, and K. B. Whaley, Phys. Rev. E **55**, 3664 (1997).
[23] A. Viel and K. B. Whaley, J. Chem. Phys. **115**, 10186 (2001).
[24] M. D. Coutinho-Neto, A. Viel, and U. Manthe, J. Chem. Phys. **121**, 9207 (2004).
[25] A. Niño and C. Muñoz-Caro, Comput. Chem. (Oxford) **19**, 371 (1995).
[26] S. Urban, R. D'Cunha, K. N. Rao, and D. Papoušek, Can. J. Phys. **62**, 1775 (1984).
[27] S. A. Chin and E. Krotscheck, Phys. Rev. B **52**, 10405 (1995).
[28] A. Viel, M. V. Patel, P. Niyaz, and K. B. Whaley, Comput. Phys. Commun. **145**, 24 (2002).
[29] R. A. Aziz, F. R. W. McCourt, and C. C. K. Wong, Mol. Phys. **61**, 1487 (1987).
[30] J. C. Light, I. P. Hamilton, and J. V. Lill, J. Chem. Phys. **82**, 1400 (1985).
[31] C. Leforestier, J. Chem. Phys. **94**, 6388 (1991).
[32] B. H. Wells, Chem. Phys. Lett. **115**, 89 (1985).
[33] M. Lewerenz, J. Chem. Phys. **104**, 1028 (1996).
[34] M. P. Hodges (private communication).
[35] P. Huang, A. Viel, and K. B. Whaley, in *Recent Advances in Quantum Monte Carlo Methods*, Recent Advances in Computational Chemistry Vol. 2, edited by W. A. Lester, Jr., S. M. Rothstein, and S. Tanaka (World Scientific, Singapore, 2002), Pt. II, p. 111.
[36] P. J. Reynolds, D. M. Ceperley, B. J. Alder, and W. A. Lester, J. Chem. Phys. **77**, 5593 (1982).
[37] M. A. Suhm and R. O. Watts, Phys. Rep. **204**, 293 (1991).
[38] V. Buch, J. Chem. Phys. **97**, 726 (1992).
[39] C. J. Umrigar, M. P. Nightingale, and K. J. Runge, J. Chem. Phys. **99**, 2865 (1993).
[40] B. L. Hammond, W. A. Lester, and P. J. Reynolds, *Monte Carlo Methods in Ab Initio Quantum Chemistry* (World Scientific, Singapore, 1994).
[41] A. Sarsa, K. E. Schmidt, and J. W. Moskowitz, J. Chem. Phys. **113**, 44 (2000).
[42] R. Assaraf, M. Caffarel, and A. Khelif, Phys. Rev. E **61**, 4566 (2000).
[43] A. Viel, M. D. Coutinho-Neto, and U. Manthe, J. Chem. Phys. **126**, 024308 (2007).
[44] M. Lewerenz, J. Chem. Phys. **106**, 4596 (1997).
[45] D. Blume and K. B. Whaley, J. Chem. Phys. **112**, 2218 (2000).